Laine, Sampo; Haikonen, Sampo; Tiainen, Tuomas; Viitala, Raine

Rotor resonance avoidance by continuous adjustment of support stiffness

Published in:
International Journal of Mechanical Sciences

DOI:
10.1016/j.ijmecsci.2024.109092

Published: 15/05/2024

Document Version
Publisher's PDF, also known as Version of record

International Journal of Mechanical Sciences 270 (2024) 109092

Contents lists available at ScienceDirect

International Journal of Mechanical Sciences

journal homepage: www.elsevier.com/locate/ijmecsci

Rotor resonance avoidance by continuous adjustment of support stiffness ☆

Sampo Laine *, Sampo Haikonen, Tuomas Tiainen, Raine Viitala

Department of Mechanical Engineering, Aalto University, P.O. Box 14300, 00076 Aalto, Finland

ARTICLE INFO

Keywords:
Rotor-bearing system
Rotor dynamics
Vibration control
Rolling element bearing
Foundation stiffness
Variable stiffness

ABSTRACT

This paper presents a method to reduce lateral vibration amplitudes in large rotating machines. The method is based on avoiding resonances by altering the natural frequencies of the rotor system at each rotating speed during operation. While many research papers have considered altering support stiffness during crossing critical speeds, continuous adjustment methods have received less attention. Continuous on-line adjustment of the natural frequencies of a rotor system is possible to a large range by adjusting the support stiffness of the bearing housings. The optimal foundation stiffness tuning policy can be defined utilizing a rotordynamic model or experimental measurements, effectively creating a resonance-free operating speed region, where vibrations are drastically reduced. It is shown through full-scale experimental laboratory tests, that the subcritical and supercritical response of the rotor system is significantly decreased during run-up and run-down with the optimal foundation stiffness tuning strategy. The developed method can be applied to reduce vibrations in any rotating machinery, where a variable foundation stiffness control can be installed. Moreover, this on-line foundation stiffness tuning strategy could also be applied in combination with resonance crossing methods involving stiffness manipulation.

1. Introduction

In many of the applications employing large flexible rotors, the operating speed is defined by the process, resulting in variable speed operation. Variable speed applications are challenging for vibration mitigation, as it is difficult to avoid resonances originating from many excitation sources. Subcritical resonances occur when the natural frequencies of a rotor system coincide with the excitation frequencies at rotating speeds below the critical speed [1]. These excitation frequencies are often harmonics of the fundamental frequency, i.e., integer multiples of the rotating speed of the rotor. Common sources of excitations observed at some integer multiples of the fundamental frequency include mass unbalance, misalignment, rolling-element bearings [2–7], gears, process machinery and rotor asymmetry [8,9]. Subcritical resonances may also be caused by excitations at non-integer multiples of the rotating speed, such as those originating from defects in rolling-element bearings [10]. In variable speed machinery, where vibrations lead to constraints in the machine use, vibration attenuation methods are crucial.

Amplitude of resonant vibrations in a system is dependent on its damping characteristics. Bearings and support structures are typically the primary source of damping. The damping properties of the supporting structures can be enhanced through passive means, such as squeeze-film dampers, which rely on energy dissipation through viscous friction [11,12]. Squeeze film dampers can be applied together with rolling element bearings [13,14], as well as with journal bearings [15], to promote damping and stability of rotor systems. If damping of the rotor system is insufficient, passive vibration absorbers such as tuned-mass dampers can be considered. Vibration isolators, another form of passive vibration damping, aim to separate system vibrations from its surroundings. Various designs have been explored for vibration isolators [16,17]. In all these passive vibration mitigation methods, optimal damping and stiffness are considered to determine the most effective damping properties for the given system [18].

A major field of research in vibration mitigation of rotating systems is active vibration control. In contrast to passive dampers, active control methods rely on actuators to actively apply energy to counteract vibrations [19]. In most cases, the control is applied using electromagnetic [20], piezoelectric [21], or hydraulic actuators [22]. Zaccardo et al. [23] studied vibration control of flexible rotors with magnetic actuators mounted on a fluid-film bearing. Jungblut et al. [24] used piezo actuators acting on the bearing supports. The advantage of force input on the bearing supports instead of the rotor directly is the lower energy consumption. In their work, control strategy was devised, where the elastic deformation of the rotor was used as a control variable. D'amato et al. [25] investigated an observer-based tracking control strategy for rotor systems supported by fluid film bearings. The method

☆ Funding: This work was supported by Business Finland, grant number 3014/31/2021 and the Academy of Finland, Finland, grant number 346443.
* Corresponding author.
E-mail address: sampo.laine@aalto.fi (S. Laine).

https://doi.org/10.1016/j.ijmecsci.2024.109092
Received 24 November 2023; Received in revised form 6 February 2024; Accepted 6 February 2024
Available online 13 February 2024

was validated with mathematical proof and numerical simulations. As active control transfers energy directly in the controlled system, it may cause adverse effects, such as instability [26]. Despite their several advantages, active control methods are typically more complex and energy intensive in comparison to passive or semi-active vibration mitigation methods.

Semi-active vibration control differs from the active control as the control is not directly applied to the degrees of freedom of the system [27]. Semi-active vibration control relies on modifying the damping or stiffness properties of the system to tune the system response. Various constructions have been considered to enable modifying the stiffness and damping properties for the purposes of semi-active control methods [28–33]. Controllable stiffness and damping devices are used in semi-active control for both vibration isolators and vibration absorbers. Nelson et al. [34], studied skyhook damping as a means to attenuate structural vibrations of a bridge. In this feasibility study, they considered adjusting the damping properties of a variable orifice damper to tune the system response. Unlike in the case of semi-active control, in adaptive-passive systems, the stiffness or damping varies during operation without the use of a controller [35]. Adaptive-passive vibration control methods have been studied especially in the field of seismic protection [36], and vibration isolation of rotating machines [37].

It was realized already in the 90s that it is possible to reduce the vibration responses during crossing of natural frequencies by momentarily lowering the natural frequency of the system with stiffness switching devices when the system approaches resonance [38–41]. Since then, many research papers have applied the same principle for mitigating resonant vibrations. Nieto et al. [42,43], used a stiffness switching pneumatic vibration isolator to cross resonances. In [44], a simulation study was conducted on temporarily lowering the support stiffness during crossing over of critical speeds, thus limiting the time spent in resonance. Similar approach was proposed by Hu et al. [45], where numerical and experimental tests were considered to cross critical speed of a spherical superconducting rotor. Zhang et al. [46], considered a switching strategy in a simulation study to evaluate the feasibility of the resonance crossing approach in a turbojet application. Jin et al. [47] also investigated the momentary stiffness reduction in an application for suspension of a railway vehicle. The numerical results were confirmed with laboratory-scale measurements. An alternative path for mitigating resonant vibrations is acceleration scheduling [48]. In [49], a device capable of adjusting the support bearing position of a rotor was investigated in a study combining stiffness switching and acceleration scheduling. Ding et al. [50] also conducted a simulation study to investigate the stiffness switching and acceleration scheduling simultaneously.

Smart materials, including magnetorheological and electrorheological fluids, as well as shape memory alloys, have gained significant attention in the field of vibration control for rotating machines [51]. The damping properties of magnetorheological fluids can be manipulated in disk dampers to achieve optimal damping for each mode of a rotor system [52]. Greiner-Petter et al. [53] considered a mechanism based on magnetorheological fluid valves and two springs to achieve continuously adjustable damping with three different stiffness options. Magnetorheological dampers can also be applied to suppression of torsional vibrations [54], moreover, many studies have considered introducing magnetorheological fluids to squeeze film dampers [55,56]. Wang et al. [57] developed an integral magnetorheological damper, which enables the control of the magnitude and direction of the fluid film force. The control method for this damper was further extended with oil film zoning control to enhance the damping properties in high frequencies [58]. The stiffness of shape memory alloys can be manipulated by adjusting their temperature [59]. This effect can be exploited to cross resonances without any acceleration of the rotor. The resonance crossing is done by accelerating the rotor close to the resonance speed and then stopping the acceleration while the stiffness of the supports is decreased with temperature adjustment [60]. Several studies have been dedicated to improving the material properties of the shape memory alloy, as well as the configuration of the system to decrease the response amplitudes and increasing the stiffness adjustment speed [61–64], in these works, the focus has remained solely on vibration attenuation during resonance crossing.

Foundation and bearing stiffness has a major influence on the dynamics of rotating systems [65–67]. Most notably, the natural frequencies of a flexible rotor are greatly affected by the stiffness of the foundations [68,69]. While many studies have considered exploiting variable stiffness to cross resonances, only a few studies have considered continuously adjustable stiffness to completely avoid resonances. In a computational study by Homisin et al. [70], tuning method for torsional vibrations of a maritime propulsion system was proposed. Their method was based on crossing the first torsional natural frequency at a low rotating speed, and then creating a resonance free region by increasing the stiffness in proportion to the rotating speed. Unfortunately no experimental validation was presented in their research. In a preliminary computational study by Laine et al. [71], the feasibility of a continuous foundation stiffness was evaluated for large rotating systems in an application of semi-active vibration control. Tawfik [72] used a device based on continuous stiffness adjustment to tune the vibration response of a rigid rotor. In their approach, rather than optimizing the resonance crossings, an algorithm based on artificial neural network was used to tune the foundation stiffness to a value which minimizes the vibration response. Several other works have also considered continuously adjustable torsional stiffness devices for tuning torsional natural frequencies [73–75], however, these research works did not consider optimal adjustment.

This paper proposes a method for reducing lateral vibrations in rotor systems based on a foundation stiffness control device with continuously adjustable stiffness. Rather than tuning the damping as in conventional vibration absorbers, or rapidly altering the stiffness to cross resonances, the device is used to optimally alter the dynamics of the rotor system for each operating speed in a given operating speed range. At subcritical speeds, the main criteria for adjustment of the stiffness should be to limit the effect of resonances due to the predominant excitation frequencies, i.e., integer multiples of the rotating speeds. For supercritical systems, the critical speeds are the most important source of vibrations. Adjusting the foundation stiffness during operation enables avoiding resonances in a large speed range. The authors claim the following original contributions:

1. An optimization law is derived for selecting the optimal foundation stiffness at each rotating speed, which maximizes the separation margin between the natural frequencies and the harmonics of the fundamental frequency of the system.
2. A method is proposed for using the optimal foundation stiffness adjustment during operation to avoid subcritical vibrations in a variable-speed rotor system.
3. Simulation study based on a rotordynamic model is presented to validate the proposed vibration mitigation method.
4. An experimental validation of the proposed method is conducted with a full-scale laboratory test rotor. Adjustment devices integrated into the horizontal supports of the bearing housings are used to tune the foundation stiffness during operation.

The rest of the paper is structured as follows. In Section 2, the theoretical rotor system model is introduced along with the harmonic excitation model used to simulate the subharmonic resonances. Section 3 presents the optimization method used to calculate the foundation stiffness map for the tuning algorithm. Section 4 describes the experimental rotor system. In Section 5, the numerical and experimental results of the proposed vibration control method are presented and discussed. Finally, some conclusions are drawn from the results.

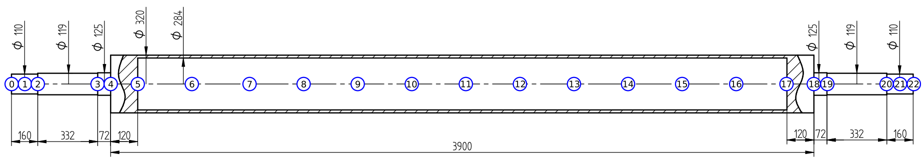

Fig. 1. Rotor dimensions and node positions. All the dimensions are in mm. The rotor system model consists of 21 Timoshenko beam elements and four point mass degrees-of-freedom of the support models. Support models, consisting of the bearings and foundations, are connected to nodes 1 and 21 of the rotor model.

2. Rotor system model

A rotordynamic model based on a laboratory test rotor is established. The rotor system model includes the rotor itself together with a model of the supporting structure. The rotor model is developed using measured geometrical dimensions, while the support models are based on experimental measurements. This rotor model is used later as a basis when the optimal tuning method is developed. The rotor model consists of 21 Timoshenko beam elements. The rotor dimensions and node positions are given in Fig. 1.

The system model can be written in matrix form with the equations of motion

$$\mathbf{M}\ddot{\boldsymbol{x}} + (\mathbf{C} + \mu\mathbf{K} + \omega\mathbf{G})\dot{\boldsymbol{x}} + \mathbf{K}\boldsymbol{x} = \mathbf{f}, \tag{1}$$

where $\mathbf{M}$, $\mathbf{C}$, $\mathbf{G}$, and $\mathbf{K}$ are the global mass, damping, gyroscopic and stiffness matrices of the rotor system, respectively. These matrices are obtained from the finite-element model of the rotor system, these matrices include the bearing and support structure model. $\boldsymbol{x}$ is the vector of the free variables, and $\mathbf{f}$ is the forcing vector. Damping is modeled using stiffness proportional part of Rayleigh damping. The damping coefficient μ is an experimentally determined parameter. The steady-state solution to this system of equations is calculated using the receptance matrix with the assumption of harmonic excitations. The response is calculated separately at each rotating speed for each harmonic component of the excitation force, and the total response at each rotating speed is the sum of these individual responses, following the principle of superposition.

2.1. Support structure model

The effect of the supports is included in the rotor model via additional non-rotating degrees of freedom. The support models are connected to the rotor model at the bearing positions. A schematic of the support system is shown in Fig. 2. Photo of the physical setup and the equivalent spring–mass–damper model are shown in Fig. 3. The supports are asymmetric in the horizontal and vertical directions. The vertical and horizontal components are marked with the subscripts v and h, respectively. The supports consist of stiffness and viscous damping of the bearings, $k_\mathrm{b}, c_\mathrm{b}$, the equivalent mass m given in vertical and horizontal directions, as well as the equivalent stiffness and viscous damping of the foundations k_f and c_f, respectively. The support structure parameters are given in Table 1.

The bearings of the rotor rest on a cradle supported by very low stiffness plate springs. The effective horizontal support is provided by a cantilever beam, the length of which can be modified with position controlled servomotors. The total effective beam length which can be modified is 300 mm, this is referred to as the HSA (horizontal stiffness adjuster) position in the paper. The horizontal stiffness can be adjusted rapidly at any rotating speed. The devices are software limited to moving from one extreme to another in 10 s. For further technical details on the stiffness adjustment devices the reader is referred to [76].

In the model, the equivalent stiffness values of the bearings are tuned so that the lowest two natural frequencies are close to the measured ones, while the rotor model is based on geometrical dimensions. Equivalent mass of the supports is estimated from the dimensions of the bearing housings and the cradle. The damping properties of the rotor system varies between different values of foundation stiffness. The damping is applied through the stiffness proportional Rayleigh damping (cf. Eq. (1)). The damping coefficient μ is estimated by matching the dissipation rate of the first elastic mode to an estimate calculated from unbalance response measurements at the highest and lowest natural frequency condition. The estimated values of μ are 0.065 s in the high natural frequency condition and 0.015 s in the low natural frequency condition. For simplicity, it is assumed, that the damping coefficient is proportional to the first horizontal natural frequency. Numerical values used in the support structure model are given in Table 1.

Table 1
Parameters of the support structure models.

Parameter	Horizontal	Vertical	Unit
k_b	30	50	$\mathrm{MN\,m^{-1}}$
k_f	[2.75–12]	200	$\mathrm{MN\,m^{-1}}$
c_b	43	43	$\mathrm{kN\,m^{-1}\,s^{-1}}$
m	190	190	kg

Table 2
Comparison of measured and modeled natural frequencies and their relative errors.

Mode	min k_{fx}			max k_{fx}		
	Model	Measured	Error	Model	Measured	Error
1st horizontal	10.6 Hz	10.68 Hz	0.75%	18.6 Hz	18.7 Hz	0.54%
2nd horizontal	14.6 Hz	13.8 Hz	5.8%	29.1 Hz	30.0 Hz	3.0%
3rd horizontal	44.7 Hz	50.3 Hz	11.1%	53.1 Hz	55.9 Hz	5.0%
1st vertical[a]	N/A	18.8	–	N/A	18.8	–
2nd vertical	27.6	29.9	7.7%	27.6	29.9	7.7%
3rd vertical	64.0	56.3	13.7%	64.0	56.3	13.7%

[a] Structural mode which is not included in the rotor system model.

In this model, the horizontal foundation stiffness can be varied in the range of 2.75 MN/m to 12 MN/m. Adjustment is simultaneous at both bearing locations. A smaller relative change in stiffness is needed to change the natural frequencies in the lower frequency range. The foundation stiffness is always assumed to be equal in both ends of the rotor. No noticeable cross-coupling effects are present in the foundations. Comparison of the natural frequencies of the model and experimental measurements is shown in Table 2.

The first three horizontal bending modes of the rotor system are shown in Fig. 4. As expected, the mode shapes are not greatly affected by the foundation stiffness adjustment, while their respective frequencies are greatly altered. The first two modes are more sensitive to the foundation stiffness adjustment than the third mode. The difference in sensitivity is due to the amount of relative movement at the foundations, as can be confirmed in Fig. 4.

It should be noted, that several research works have linked the support asymmetry to excitation of backward whirl modes [77–81]. In most practical applications of large rotating machinery, the support stiffness is asymmetric by default, thus there is no major concern associated with increasing or decreasing this asymmetry during operation. The vibration amplitude is calculated as the maximum displacements of the rotor orbit from the origin in the horizontal direction. The present study omits detailed analysis of the whirl modes, as the primary focus is on the relative change in vibration amplitudes.

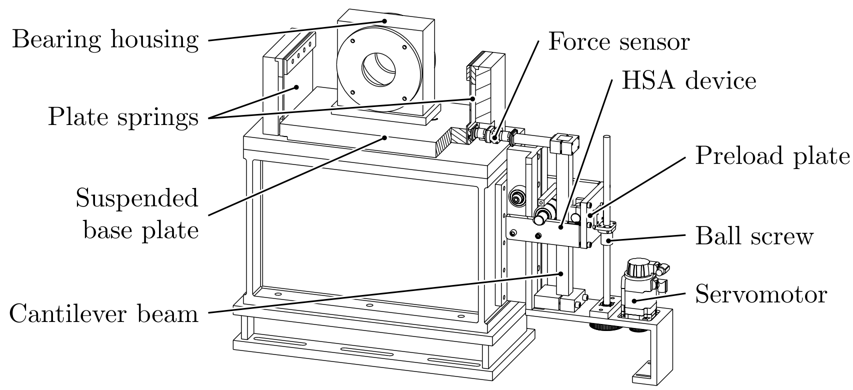

Fig. 2. Schematic of the foundation stiffness adjustment device. The bearing housing is supported by a base plate, which is suspended in the air by two horizontally flexible plate springs. Horizontal stiffness is provided by a cantilever beam, the effective height of which can be controlled with the horizontal stiffness adjuster (HSA) device. The structure is identical at both bearing locations.

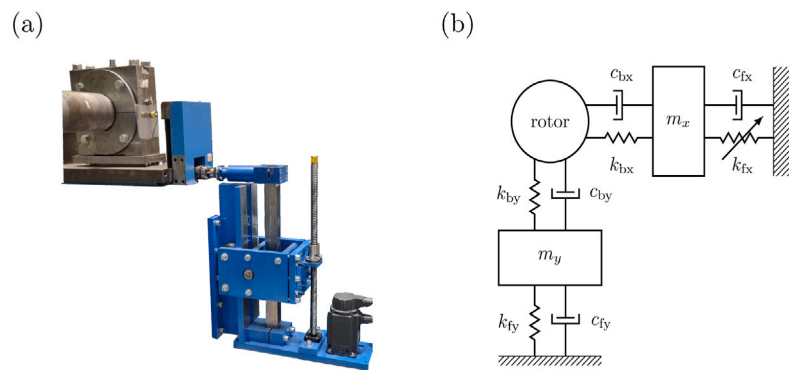

Fig. 3. Support structure model. The laboratory setup is seen in (a), and the equivalent model in (b). The equivalent model consists of the non-rotating degrees of freedom in horizontal and vertical directions, the bearing stiffness and damping k_b, c_b, and the foundation stiffness and damping, k_f, c_f. The foundation stiffness can be controlled in horizontal direction with the horizontal stiffness adjuster device.

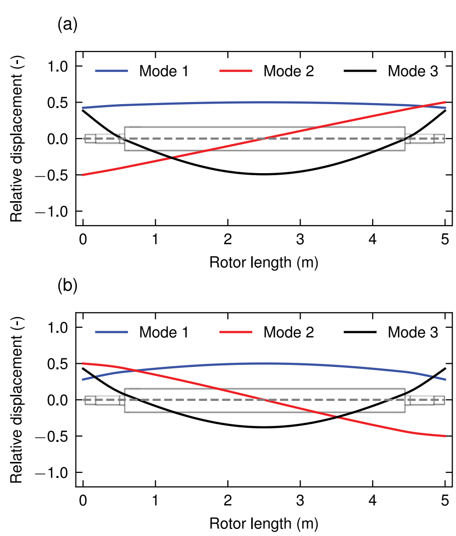

Fig. 4. Three lowest horizontal bending modes of the rotor system model. The mode shapes at minimum foundation stiffness are shown in (a) and with maximum foundation stiffness in (b). When minimum foundation stiffness is applied, there is less bending especially in the modes 1 and 2 when compared to the high stiffness case. The decrease in the foundation stiffness is associated with less bending of the rotor and increased displacement in the supports. The natural frequencies associated with these mode shapes are given in Table 2.

2.2. Excitation model

The primary source of excitation in rotating machines is unbalance, where the axis of rotation deviates from the axis of the mass centroid. Balancing is performed to decrease the amount of unbalance, but it can never be completely eliminated. The frequency of the excitation caused by unbalance is equal to the rotating speed. When the rotating machine is operated below the critical speed, resonances caused by higher order harmonics become significant source of vibration. The unbalance excitation is described by the equation

$$F_{\mathrm{ub}}(t) = \mathrm{Re}\left[m\epsilon\omega^2 e^{j(\omega t+\phi_{\mathrm{ub}})}\right], \tag{2}$$

where F is the unbalance force, m is the unbalance mass, ϵ is the distance of the unbalance mass from the axis of rotation, ϕ_{ub} is the phase of each excitation, ω is the rotating speed, j is the imaginary number and $\mathrm{Re}[\cdot]$ denotes the real part of complex number. The location for the excitation in the rotor model should be chosen so that all the modes of interest are excited. In this paper, we focus on the three lowest lateral modes. Modal analysis reveals that by applying the excitation to node 7 of the rotor model, all these modes of interest can be effectively excited. The 1x harmonic of the excitation force is calculated by assuming an unbalance mass of 500 g at 10 cm distance from the axis of rotation.

Many models have been proposed for modeling the excitations caused by rolling element bearings [82]. Significant proportion of the harmonic excitations caused by rolling-element bearings can be attributed to the roundness profile of the bearing inner race [9]. Other sources include misalignment [83], contacts and deformation [84], and outer race waviness [85]. To model the most significant sources of

Table 3
Horizontal force components of the bearing excitations calculated by Choudhury et al. [7].

Waviness component n	Non-drive end		Drive end	
	A_n (μm)	ϕ_n (deg)	A_n (μm)	ϕ_n (deg)
1	0.76	123.8	0.06	179.6
2	13.18	273.7	5.24	356.4
3	5.57	182.5	1.67	141.8
4	7.367	265.5	1.63	213.3

vibrations, while preserving reasonable simplicity of the model, the bearing excitation is calculated according to the base excitation method proposed by Choudhury et al. [7]. The excitation parameters (Table 3.), which were applied in the analyses were determined in the previous study, where the measured bearing inner race geometries were used as an input to a bearing kinematic model. The forced movement of the rotor transferred to the rotor through the bearing stiffness and damping. The total base excitation due to the inner ring waviness can be presented in the complex form as

$$F_{\mathrm{bw}}(t) = \mathrm{Re}\left[\sum_n A_{\mathrm{n}}(k_{\mathrm{b}} + jc_{\mathrm{b}}n\omega)e^{j(n\omega t+\phi_n)}\right] \tag{3}$$

where A_n and ϕ_n are the amplitude and phase of the n:th bearing excitation component. Here the excitations are considered up to the fourth order. This model is preferred over more complex bearing kinematic models, as the steady-state solution can be directly calculated without numerical integration, while preserving a fair accuracy of the response [7].

3. Optimal foundation stiffness tuning method

This section presents the proposed vibration control method. The principle of the resonance avoidance is to increase the separation margin between the most important excitations and the natural frequencies of the rotor during operation based on an optimal mapping. In contrast to methods considering crossing the resonances by momentarily lowering the foundation stiffness [42–44,46,47], the proposed method relies on continuous foundation stiffness adjustment to avoid the resonances in a pre-defined operating speed range. These resonances are completely eliminated in the optimization range by adjusting the foundation stiffness as the operating speed varies.

The optimality condition is based on maximizing the separation margin between the fundamental frequency and integer fractions of the natural frequencies at each rotating speed. The system natural frequencies must be known as function of the foundation stiffness adjustment for the optimization. In this study, a rotordynamic model and impulse response tests were used to define the three lowest natural frequencies of the rotor system. The measurements were conducted at stationary condition for each foundation stiffness value (Fig. 6). A fourth order polynomial function was then fit to the measurements to obtain a continuous mapping from the chosen foundation stiffness set point to the natural frequencies of the system. In the simulation cases, the natural frequencies were calculated directly from the eigenvalues of the system matrix each time the foundation stiffness is modified.

The optimal foundation stiffness mapping is based on accelerating with minimum foundation stiffness until the chosen excitation frequency crosses the first natural frequency. After the resonance is crossed, the separation margin between the chosen excitation and the two lowest natural frequencies are maximized. The largest possible separation margin can be achieved by minimizing the difference between the avoided excitation frequency and the natural frequencies of the rotor system. The optimization problem can be written for an arbitrary excitation frequency as

$$\begin{aligned}
\min_{k} \quad & w|f_{\mathrm{ex}}(\omega) - \lambda_1(k,\omega)| - (1-w)|f_{\mathrm{ex}}(\omega) - \lambda_2(k,\omega)| \\
\text{s.t.} \quad & f_{\mathrm{ex}}(\omega) - \lambda_1(k,\omega) > 0, \\
& f_{\mathrm{ex}}(\omega) - \lambda_2(k,\omega) < 0, \\
& k_{\mathrm{min}} \le k \le k_{\mathrm{max}}, \\
& 0 < w < 1,
\end{aligned} \tag{4}$$

where $f_{ex}(\omega)$ is the excitation frequency at a given operating speed ω, and λ_1 and λ_2 are the first and second natural frequencies of the system. The foundation stiffness value k which minimizes this problem maximizes the separation margin from the excitation to the natural frequencies. The optimization weight w can be used to adjust the relative distance from the two resonances. In the following, value of 0.5 is used for the weight parameter to set the distances equal. The excitation frequency f_{ex} can be an integer or non-integer multiple of the rotating frequency. The additional constraints enforce that the excitation frequency of interest never crosses the natural frequencies in the optimization range.

The choice of the excitation frequencies to be avoided depends on the application. The optimization range is limited by the maximum natural frequency adjustment that can be achieved by modifying the foundation stiffness, which in turn depends on the design of the rotor. The maximum theoretical adjustment range can be analyzed with a rotordynamic model by varying the support stiffness from zero to infinity. After the analysis, an adjustment device can be designed in accordance to the desired operating speed range.

In this paper, two speed range cases are considered. The two cases are the lower speed subcritical vibration case, where the optimization is done for the 2x harmonic of the fundamental frequency, and a higher speed supercritical case, where the optimization is done for the fundamental frequency, i.e., the 1x harmonic. The optimization problem is defined in a way that the resonances corresponding to these excitations are avoided in the operating speed range. The resonances are passed at the lowest possible operating speed, where the excitation power is smaller, as long as the damping of the system is not compromised by lowering the foundation stiffness. After crossing of the resonances, optimal adjustment of the foundation stiffness then allows for effectively extending the resonance-free operating speed range. The optimal natural frequencies for both cases are illustrated in a diagram shown in Fig. 7.

In the present study, impulse response tests were conducted to estimate the natural frequencies of the system at each applied foundation stiffness value. It should be noted, that while the impulse response tests performed in static conditions are sufficient for this application, in the case of high-speed machinery or overhung rotors, the gyroscopic effect can significantly influence the natural frequencies. Thus, in those cases, a refined rotordynamic model or measurements in operating conditions should instead be used to evaluate the natural frequencies.

4. Experimental study

This section describes the used experimental hardware and the measurement instrumentation. The test rotor was a 720 kg paper machine guidance roll. The roll was supported by rolling-element bearings. The measurement setup is displayed in Fig. 5. The test rotor is an example of a flexible rotor, which exhibits several distinct bending and conical modes during operation. The basis of the test-bench is a modified roll grinder. The rotor was balanced using two balance planes before the measurements.

Continuous adjustment of the horizontal foundation stiffness was made possible in both ends of the rotor using a special research device presented in Fig. 3. The horizontal foundation stiffness was modified

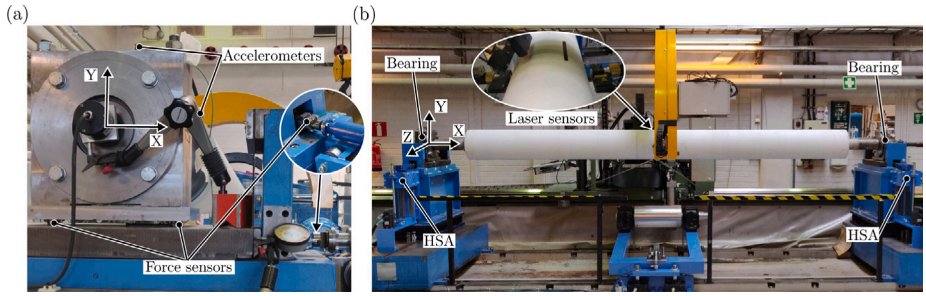

Fig. 5. Test equipment used in the laboratory measurements. The non-drive end bearing is seen in figure (a), along with the accelerometers as well as the force sensors. The whole rotor system is shown in (b), where the HSA (horizontal stiffness adjuster) devices, which are used to control the foundation stiffness, are located on both the bearing housings. The laser displacement sensors are positioned near the middle of the rotor on the arch.

by adjusting the vertical position of the HSA (Horizontal Stiffness Adjuster), which alters the horizontal stiffness of the supporting structure of the bearing housings. Moving the HSA beam support down decreases the stiffness; on the other hand, higher HSA beam support position increases the stiffness. A possible drawback of the moving contacts in the devices is the possibility of backlash. An effort was made to negate potential backlash problems by pre-loading all moving contacts, i.e., the rollers of the HSA devices. A more detailed explanation of the construction of the devices is given in [76].

Acceleration sensors mounted in vertical and horizontal direction on the bearing housings were used in the impulse response tests. The used accelerometers were Brüel & Kjær type 4381, which had maximum peak amplitude of 2000 g, sensitivity of 10 pC/ms^{-2} and bandwidth of 0.1 Hz to 4800 Hz. A total of four acceleration sensors were used, two on each bearing housings. In the run-up test a total of six force sensors, were used to measure the lateral bearing forces. Three of the force sensors were mounted in each of the supports, two measuring the vertical force and one measuring the horizontal force. The locations of the sensors are presented in Fig. 5. The horizontal force sensors were Kistler 9001A, which had a measuring range of 0 N to 7.5 kN and sensitivity of 4.3 pC N^{-1}. The vertical force sensors were HBM PaceLine CFW, which had a measuring range from 0 N to 100 kN and sensitivity of 4.3 pC N^{-1}. Additionally, the displacement of the horizontal motion of the roll was measured at position 2 m from the end of the non-drive end bearing. Matsushita NAIS LM 300 laser sensors were used. The sensors had a measurement range from 27 mm to 33 mm and a sensitivity of 1 V mm^{-1}.

The rotor was rotated by an induction motor drive. Position-servo-motors were used to adjust the beam supports in both the HSA devices. A control program written in LabView was used to perform the control system integration. Data acquisition from the sensors was done using a National Instruments PCI-6259 data acquisition card. The used sampling frequency was 5 kHz. These settings can be considered adequate for measuring vibrations with frequencies lower than 200 Hz. Kistler type 5165A4 and type 5073A charge amplifiers were used to convert the charge signals to voltage signals from accelerometers and force sensors, respectively. Amplifiers for the force and acceleration sensors were equipped with analog anti-aliasing filters with cutoff frequency of 200 Hz. The analog output of the laser sensors was antialiasing filtered with cutoff frequency of 2000 Hz.

A series of impulse response tests was performed to identify the vertical and horizontal natural frequencies of the rotor system. Due to the highly asymmetric foundations, the natural frequencies of the rotor are different in horizontal and vertical directions. The rotor was hit with a hammer at several foundation stiffness states. The tests were carried out in two separate measurements, one for the horizontal and one for the vertical direction. The rotor was stationary and supported by the bearings during the test. Fig. 6 displays the spectrograms of the impulse response at each foundation stiffness instance. As expected, the vertical natural frequencies of the rotor are not affected by the horizontal foundation stiffness adjustment. The horizontal natural frequency is

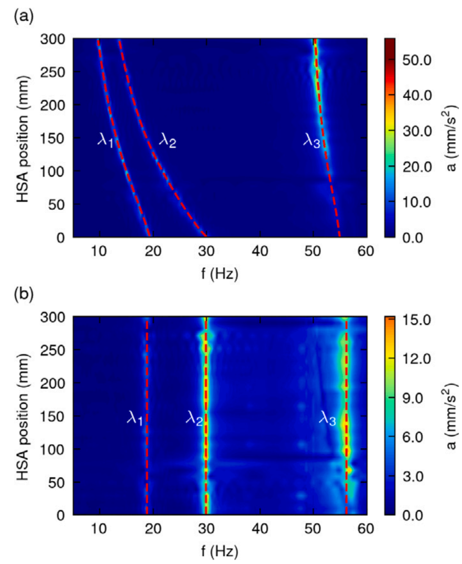

Fig. 6. Spectrogram of the impulse response tests in (a) horizontal direction, (b) vertical direction. The position of the horizontal stiffness adjuster is varied, causing a shift in the horizontal natural frequencies λ_1, λ_2 and λ_3, of the rotor system. The dashed lines correspond to fourth-order polynomial functions least-squares fit to the peak values of the spectrum at each HSA (horizontal stiffness adjuster) position. The horizontal natural frequencies are greatly altered while the vertical natural frequencies remain constant, confirming that these frequencies are uncoupled.

proportional to the horizontal foundation stiffness. These experimentally determined values are compared to the model in Table 2. A large deviation is seen in the horizontal natural frequencies, indicating that the subcritical resonance speeds can be shifted to a large extent. Peak values of the responses corresponding to the three lowest horizontal modes were detected at each HSA position. A curve fit to this data provides a mapping from the position of the HSA to the horizontal natural frequencies of the rotor system.

The optimization procedure given in Eq. (4) was applied to the identified natural frequencies. In the case of this experimental measurement, the HSA position was used as an input to the servo motors controlling the foundation stiffness adjusting devices. A Campbell diagram of the rotor system, seen in Fig. 7 is used to visualize the optimal natural frequencies which are selected for each rotating speed in the lower speed subcritical case and in the higher speed supercritical case. The figure shows the natural frequencies without optimization, when the stiffness is kept at maximum, and with the optimal foundation stiffness, where the optimal foundation stiffness is updated at each rotating speed to maximize the separation margin to the respective excitation.

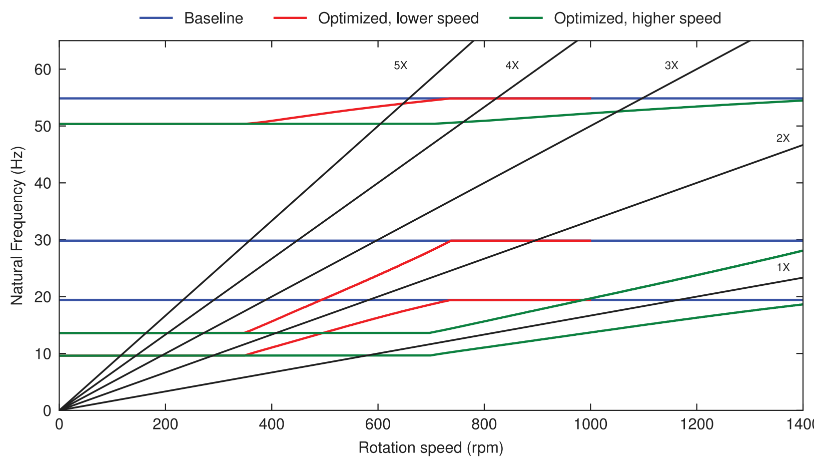

Fig. 7. Campbell diagram of the experimental system. The optimal natural frequency maps are displayed for the lower speed subcritical case, and higher speed supercritical case. In the baseline case, the support stiffness remains constant. The diagonal lines correspond to the first five harmonics of the rotating frequency.

5. Results and discussion

The effectiveness of the developed vibration mitigation method was studied by means of numerical and experimental analyses. The studied system is a rotor test-bench with a paper machine roll, supported by cylindrical rolling element bearings. In the simulation study, the optimal foundation stiffness mapping used in the control is derived directly from the model. In the experimental study, the optimal natural frequency mapping was calculated using the natural frequencies estimated from impulse response tests performed at standstill.

5.1. Simulated steady-state responses

Simulated steady-state responses are studied to evaluate the effectiveness of the developed foundation stiffness control method. The simulated responses are based on the excitation model, applied to the rotor model, both of which are detailed in Section 2. The steady-state response is then calculated at each rotating speed from Eq. (1). The response for each of the harmonic component of the excitation is calculated separately and summed to get the total displacement response orbits.

Two cases are considered in the simulation. A subcritical machine with operating speed range from 400 to 720 rpm, and a supercritical machine with operating speed range from 720 to 1400 rpm. Results of the simulation study are shown in Fig. 8. The optimal foundation stiffness tuning was applied to the rotor model by adjusting the horizontal foundation stiffness according to the optimal foundation stiffness mapping. In the lower speed case, the optimization is applied to the 2x excitation, and in the higher speed case on the 1x excitation. The optimal mapping from rotating speed to foundation stiffness is defined by solving the optimization problem in Eq. (4) for each rotating speed in the optimization range. The natural frequencies were calculated directly from the eigenvalues of the rotor system model. The optimization problem was solved using Powell's method.

In the lower speed simulation case (Fig. 8), the total vibration amplitudes corresponding to the subcritical resonances are significantly decreased when the optimal foundation stiffness is applied. The resonances are shifted to lower rotation speeds, where they are crossed before reaching the operating speed range. In the optimized response, all resonances due to the interceptions of the excitation frequencies and the two lowest natural frequencies are eliminated in from approximately 320 rpm to 800 rpm. The resonance due to the 2x excitation is crossed at approximately 320 rpm in the optimized response. The resonance due to the 3rd natural frequency and the 5x excitation is still present, as the higher order modes are not considered by the optimization. According to this simulation, the relative amplitude of the shifted resonance peaks are also smaller when the optimization is applied, as they are crossed with less excitational energy at the lower speed.

In the higher speed case (Fig. 8), the reductions in vibration amplitudes are greater than in the lower speed case. Again, the resonances due to the two lowest modes are eliminated in the operating speed region, resulting in significant vibration attenuation at the optimization range from 780 to 1400 rpm. The first critical speed is now crossed approximately 550 rpm. The amplitude of vibrations in all resonance crossings are decreased when they occur at lower rotating speeds. Mean and maximum vibration attenuation values in the optimization range are given in Table 4.

Based on these results, the considered approach is effective in creating a resonance-free region in the chosen speed range. This is especially useful in variable-speed machines, where the rotating speed varies during operation, and in machines that need a strategy to pass the critical speeds. Choosing the excitation to avoid is based on the desired resonance-free operating speed. For high speed application, it could even be beneficial to use the 3rd and 2nd natural frequency in the optimization instead of the 1st and 2nd. In this case, the second critical speed of the rotor system would also be crossed. Additional optimization possibilities could also open if the rotor system itself can be modified. If the rotor system can be modified, the crossover of the critical and subcritical speeds could be selected more freely.

5.2. Experimental verification

Two run-up experiments were performed, one for the lower and one for the higher speed case. The acceleration time was 450 s to reach 700 rpm in the lower speed case, and 110 s to reach 1380 rpm in the higher speed case. The slow acceleration speed was chosen in the lower speed case to ensure that the subcritical resonances are clearly distinguishable in the measurements. Corresponding baseline measurements with equal acceleration times were performed using maximum support stiffness without optimization during the acceleration.

Considering the lower speed subcritical vibration case, the filtered horizontal rotor displacement and bearing force amplitudes are displayed in Fig. 9. In addition to the anti-aliasing filters used in the measurements, low-pass filtering was applied in post processing for all signals with a cutoff frequency of 200 Hz. Window length of 1000 samples was used for the peak-to-peak filter. The windowed peak-to-peak value divided by two to approximate the vibration amplitude. The displacement measurement was located 2 meters from the non-drive end bearing, while the bearing force was measured from the bearing

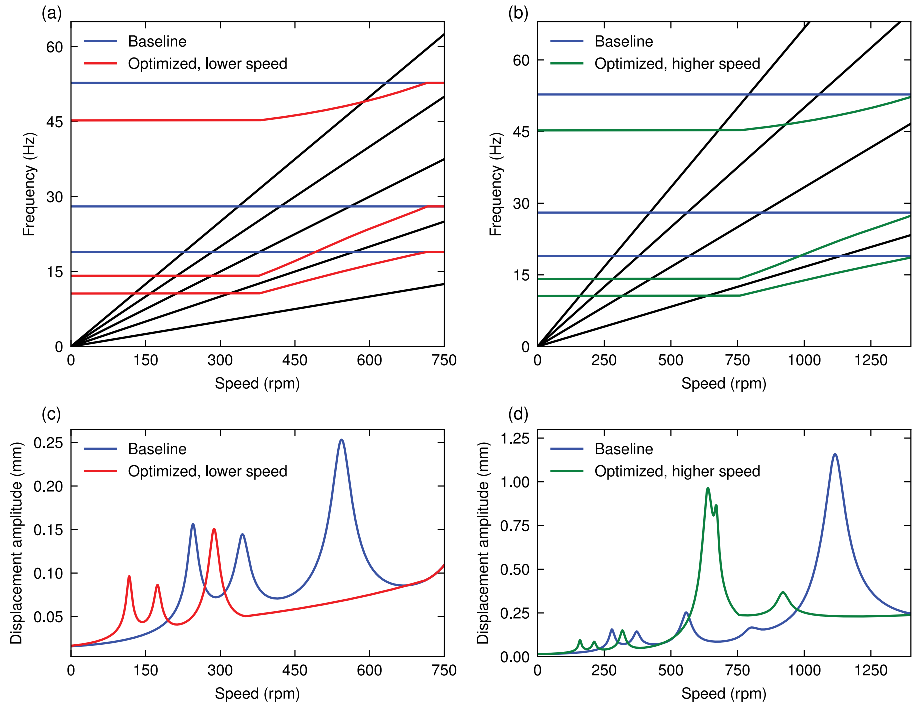

Fig. 8. Simulated responses. Optimal foundation stiffness maps are applied to shift the subcritical resonances to lower rotating speeds, as seen in the resonance interference diagrams (a) and (b). The horizontal steady-state response is calculated at the center of the rotor for each rotating speed, figures (c) and (d). The resonances due to the two lowest modes are eliminated in the operating speed region, where the foundation stiffness is adjusted based on the optimal mapping.

Table 4
Comparison of vibration amplitudes in the vibration mitigation results in the optimization range of each case.

Measurement	Subcritical		Supercritical		Unit
	Simulation	Measured	Simulation	Measured	
Mean baseline displacement	0.11	0.081	0.42	0.35	mm
Mean optimized displacement	0.067	0.057	0.24	0.17	mm
Relative mean Improvement	41.2	43.0	39.8	49.0	%
Maximum peak reduction	73.1	64.7	80.0	94.0	%

pedestal. For this reason, the resonances which are due to bending modes are predominant in the displacement measurement, while the conical modes are more clearly visible in the force measurements. Effect of the foundation stiffness control is nevertheless similar in both of the measurement locations. In the baseline measurement, vibration peaks are present at subcritical resonances during multiple points of the run-up. To ensure that the subcritical resonances are clearly visible in the data, the acceleration of the rotor was performed in a step-wise fashion, with 5 s interval between each acceleration step. For this reason, small force spikes are observed in the bearing force corresponding to these acceleration times.

Results from the same bearing force measurements during the lower speed run-up are shown in a spectrogram in Fig. 9. The subcritical resonances can be clearly seen at the three lowest natural frequencies. At the baseline measurements, these natural frequencies are approximately 18.7 Hz, 30.0 Hz, and 55.9 Hz. Applying the optimal foundation stiffness effectively eliminates the resonances in the control range. The signal visible at exactly 50 Hz in the measurements is due to network disturbance, this error is constant in all operating points and does not interfere with the results. A notch filter was chosen not to be used, as the frequency is close to the third natural frequency. In the baseline measurements, the subcritical resonances corresponding to the crossings of the natural frequencies and the integer multiples of the rotating speeds are evident. In addition to the excitations visible at the integer multiples of the rotation speed, there are also excitations at non-integer multiples of the rotating speed. Upon closer inspection, it can be concluded that these non-integer excitations correspond to well-known bearing frequencies, namely, the integer multiples of the fundamental train frequency. A significant vibration peak is seen at the crossing of 5x excitation of the fundamental train frequency at approximately 510 rpm. This result implies, that for systems employing rolling element bearings, the excitations arising from the bearing defects can be significant. If a major resonance due to a non-integer frequency was detected after applying the optimization, it could be mitigated by adjusting the weight parameter w in the optimization Eq. (4).

The results of the higher speed supercritical vibration case are shown in Fig. 10. The results are shown as the windowed peak to peak amplitude of horizontal displacement and vibration speed at the midpoint of the rotor. Vibration speed is calculated by numerical differentation of the displacement measurement. Control of the foundation stiffness during the run-up and coast down effectively eliminates the resonance due to the horizontal bending mode in the optimization range. The vibration amplitudes are decreased by an order of magnitude in the optimization region. The critical speed is shifted to a significantly lower frequency, which enables crossing the critical speed at the lower speed. The second critical speed is never reached, as the natural frequency increases together with the operating speed.

The effectiveness of the vibration attenuation is analyzed with in the operating speed range in both cases. Table 4 shows the mean displacement amplitudes calculated as the mean value of the windowed vibration amplitude in the respective optimization range. The relative mean improvement is the percentage which the mean value decreases when the optimal foundation stiffness is applied. As expected, the mean vibrations decrease in both experiments. Same values calculated from the simulation results are in alignment with the experiments. The maximum peak reduction is calculated as the maximum vibration reduction

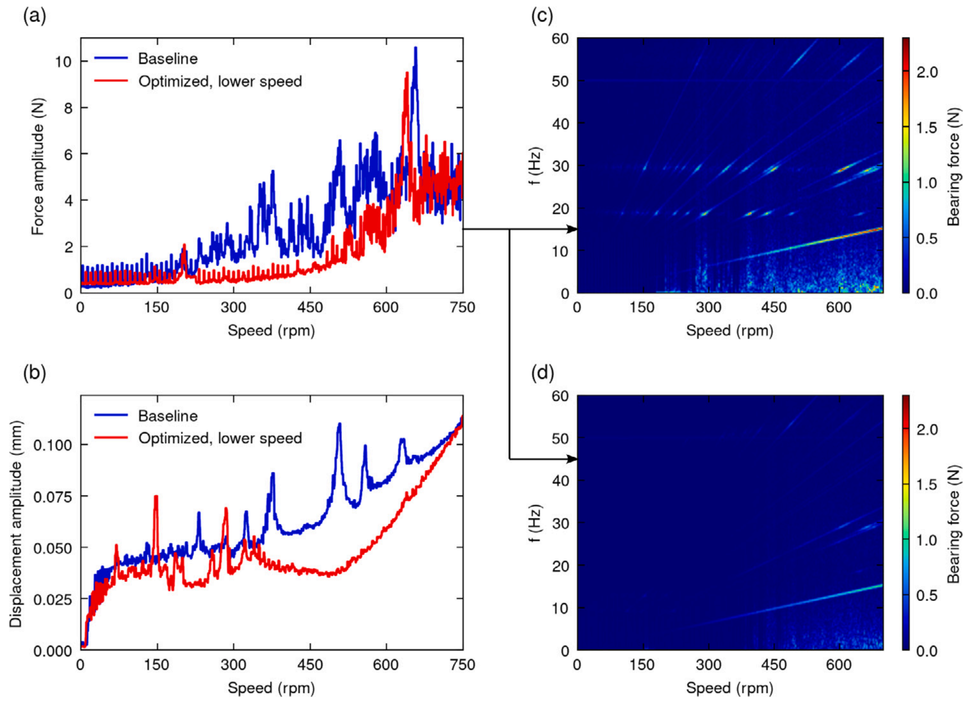

Fig. 9. Experimental run-up tests. The total displacement amplitudes calculated from the subcritical measurements are shown in (a), while the amplitude of the bearing force measured from the bearing is shown in (b). In this lower speed case, the rotating speed is increased every five seconds, which explains the comb-like peaks visible in the force measurements. Decrease of vibrations is visible in both measurements in the optimization range from 300 rpm to 700 rpm. Panels (c-d) show the spectrograms calculated from the bearing force signals. The baseline run-up is shown in (c) and the optimized run-up in (d). The subcritical resonances are visible at the natural frequencies in the baseline case, these resonances are shifted to lower speeds and hardly visible in the optimized run-up.

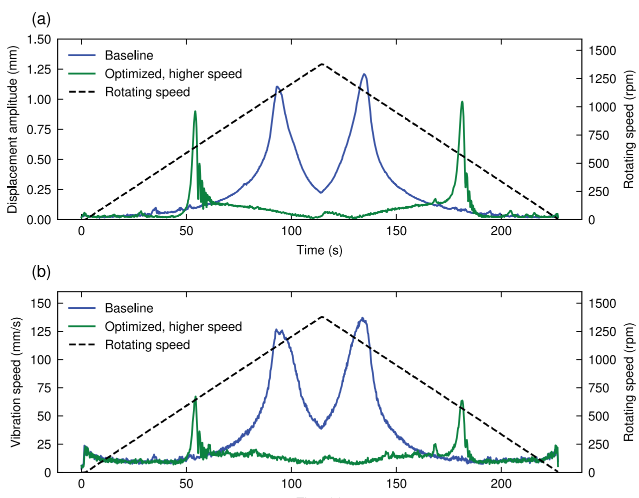

Fig. 10. The higher speed run-up and coast-down case. The windowed horizontal peak-to-peak vibration of the centerpoint of the rotor is seen in terms of displacement (a) and vibration speed (b). The horizontal resonances are effectively eliminated in the optimization regime during 70 to 170 s.

that is achieved in the optimization range, this value corresponds to the best case scenario for the optimization, where the baseline vibration is at the highest resonance point, which is eliminated by the optimization. In the lower speed case, this most significant vibration peak is the 5x resonance of fundamental train frequency at approximately 510 rpm. In the higher speed case, the most significant vibration peak is the critical speed. The measurements show, that the optimization leads up to 94 percent decrease in the peak vibration in the supercritical case. The measured improvements with the vibration control method are slightly higher than anticipated by the theoretical model. The differences between the modeled and measured results are minor.

The developed optimal foundation stiffness tuning method's reliability and robustness, wide operating range, and direct applicability for large-scale operation make it an interesting option compared to contemporary active or semi-active vibration control methods. The chosen target function which maximizes the separation margin is a simple but robust approach for mitigating resonant vibrations. More complex target functions, such as one minimizing a simulated response would be sensitive to modeling inaccuracies, since even a small inaccuracy in the model can compromise the separation margin. Although the used actuators are not suitable for fast dynamic control, such as active vibration control, it is still possible to achieve significant vibration attenuation. The proposed method may have applications, for example, in the paper industry, where large flexible rotors are commonly used, and minor rotor vibrations can have a direct influence on the production quality. Various requirements and process parameters govern the optimal rotating speed of rolls, and rotors may end up running at a speed coinciding with a subcritical resonance frequency. Furthermore, in some machinery such as winders, the natural frequencies of the system change during operation. The proposed method could be especially suitable for application in this kind of machinery.

6. Conclusions

In this paper, a vibration mitigation method based on optimally tuned foundation stiffness was presented for resonance avoidance in rotating systems. The foundation stiffness of the rotor is continuously adjusted during operation, effectively creating a resonance-free speed region, where resonances due to the lowest natural frequencies are eliminated. The proposed control method is compatible with resonance crossing strategies, where the stiffness is momentarily lowered during resonance crossings. A theoretical model was used to demonstrate the principle of the proposed control method, and full-scale experiments were performed to verify the results and show the effectiveness of the control method in laboratory settings on a 720 kg rotor. Measurements were performed in subcritical and supercritical operating conditions up to 1400 rpm. The foundation stiffness adjustment was implemented with research devices, which can be used to adjust the lowest horizontal natural frequency of the rotor continuously between 10.7 Hz to 18.7 Hz independently from the vertical direction.

When the rotor displacement amplitudes were measured against the baseline in run-up experiments, overall mean vibration amplitude reduction of approximately 43% was observed in the optimization range in the subcritical experiment, and 49% in the supercritical experiment. In both instances, the theoretical model exhibited a vibration attenuation performance comparable to that observed in the experiments. Bearing excitations were established as the source for the resonances in the subcritical speeds, while the resonances due to unbalance forces were dominant in the supercritical experiments. Bearing kinematics augmented base excitation method was used to model the bearing excitations at integer harmonics of the rotating frequency. The control method was effective in suppressing resonant vibrations due to integer and non-integer multiples of the rotating frequency. It was confirmed, that the observed non-integer frequencies corresponded to the harmonics of the fundamental train frequency of the rolling-element bearings.

Comparison of the theoretical and experimental results revealed that the established rotor-bearing model was able to reproduce the dynamic characteristics of the optimized rotor system. In the presented vibration mitigation method, the energy required for the actuators is negligible since the servomotors must be re-positioned only when the rotating speed changes. The used device could benefit from an additional damping element for even better vibration attenuation, especially at the low stiffness resonance crossings. Some additional considerations are required when the vibration mitigation method is implemented in industrial applications, namely, the adjustment principle should be simultaneously applied in vertical and horizontal directions.

CRediT authorship contribution statement

Sampo Laine: Writing – original draft, Visualization, Validation, Software, Methodology, Investigation, Funding acquisition, Formal analysis, Conceptualization. **Sampo Haikonen:** Writing – review & editing, Investigation. **Tuomas Tiainen:** Writing – review & editing. **Raine Viitala:** Writing – review & editing, Supervision, Project administration, Funding acquisition.

Declaration of competing interest

The authors declare that they have no known competing financial interests or personal relationships that could have appeared to influence the work reported in this paper.

Data availability

Data will be made available on request.

References

[1] Viitala R, Widmaier T, Kuosmanen P. Subcritical vibrations of a large flexible rotor efficiently reduced by modifying the bearing inner ring roundness profile. Mech Syst Signal Process 2018;110:42–58. http://dx.doi.org/10.1016/j.ymssp.2018.03.010.

[2] Wardle FP. Vibration forces produced by waviness of the rolling surfaces of thrust loaded ball bearings part 1: Theory. Proc Inst Mech Eng C 1988;202(5):305–12. http://dx.doi.org/10.1243/PIME_PROC_1988_202_127_02.

[3] Wardle FP. Vibration forces produced by waviness of the rolling surfaces of thrust loaded ball bearings part 2: Experimental validation. Proc Inst Mech Eng C 1988;202(5):313–9. http://dx.doi.org/10.1243/PIME_PROC_1988_202_128_02.

[4] Jang GH, Jeong SW. Nonlinear excitation model of ball bearing waviness in a rigid rotor supported by two or more ball bearings considering five degrees of freedom. J Tribol 2002;124(1):82–90. http://dx.doi.org/10.1115/1.1398289.

[5] Jang G, Jeong S-W. Vibration analysis of a rotating system due to the effect of ball bearing waviness. J Sound Vib 2004;269(3–5):709–26. http://dx.doi.org/10.1016/S0022-460X(03)00127-5.

[6] Liu W, Zhang Y, Feng Z-J, Zhao J-S, Wang D. A study on waviness induced vibration of ball bearings based on signal coherence theory. J Sound Vib 2014;333(23):6107–20. http://dx.doi.org/10.1016/j.jsv.2014.06.040.

[7] Choudhury T, Kurvinen E, Viitala R, Sopanen J. Development and verification of frequency domain solution methods for rotor-bearing system responses caused by rolling element bearing waviness. Mech Syst Signal Process 2022;163:108117. http://dx.doi.org/10.1016/j.ymssp.2021.108117.

[8] Bishop RED, Parkinson AG, Barlow HEM. Second order vibration of flexible shafts. Philos. Trans. R. Soc. London. Ser. A, Math. Phys. Sci. 1965;259(1095):1–31. http://dx.doi.org/10.1098/rsta.1965.0052.

[9] Viitala R. Minimizing the bearing inner ring roundness error with installation shaft 3D grinding to reduce rotor subcritical response. CIRP J. Manuf. Sci. Technol. 2020;9. http://dx.doi.org/10.1016/j.cirpj.2020.05.002.

[10] Xu H, Yang Y, Ma H, Luo Z, Li X, Han Q, et al. Vibration characteristics of bearing-rotor systems with inner ring dynamic misalignment. Int J Mech Sci 2022;230:107536. http://dx.doi.org/10.1016/j.ijmecsci.2022.107536.

[11] Gheller E, Chatterton S, Vania A, Pennacchi P. Squeeze film damper modeling: A comprehensive approach. Machines 2022;10(9). http://dx.doi.org/10.3390/machines10090781.

[12] Zheng W, Pei S, Zhang Q, Hong J. Experimental and theoretical results of the performance of controllable clearance squeeze film damper on reducing the critical amplitude. Tribol Int 2022;166:107155. http://dx.doi.org/10.1016/j.triboint.2021.107155.

[13] lun Zhou H, huo Luo G, Chen G, Wang F. Analysis of the nonlinear dynamic response of a rotor supported on ball bearings with floating-ring squeeze film dampers. Mech Mach Theory 2013;59:65–77. http://dx.doi.org/10.1016/j.mechmachtheory.2012.09.002.

[14] Yang X, Jiang B, Li Y, Zhao Q, Deng S, Zhang W, et al. Dynamic characteristics of elastic ring squeeze film damper coupled high-speed ball bearings. J Sound Vib 2022;537:117186. http://dx.doi.org/10.1016/j.jsv.2022.117186.

[15] Zeidan FY, Andres LS, Vance JM, et al. Design and application of squeeze film dampers in rotating machinery. In: Proceedings of the 25th turbomachinery symposium. Texas A&M University. Turbomachinery Laboratories; 1996.

[16] Wang S, Wang Z. Curved surface-based vibration isolation mechanism with designable stiffness: Modeling, simulation, and applications. Mech Syst Signal Process 2022;181:109489. http://dx.doi.org/10.1016/j.ymssp.2022.109489.

[17] Deng J, Yang J, Jiao S, Long X. Band-stop characteristics of a nonlinear anti-resonant vibration isolator for low-frequency applications. Int J Mech Sci 2023;240:107914. http://dx.doi.org/10.1016/j.ijmecsci.2022.107914.

[18] Heidari H, Safarpour P. Optimal design of support parameters for minimum force transmissibility of a flexible rotor based on H∞ and H2 optimization methods. Eng Optim 2018;50(4):671–83. http://dx.doi.org/10.1080/0305215X.2017.1351560.

[19] Breńkacz Ł, Witanowski Ł, Drosińska-Komor M, Szewczuk-Krypa N. Research and applications of active bearings: A state-of-the-art review. Mech Syst Signal Process 2021;151:107423. http://dx.doi.org/10.1016/j.ymssp.2020.107423.

[20] Lusty C, Keogh P. Active vibration control of a flexible rotor by flexibly mounted internal-stator magnetic actuators. IEEE/ASME Trans Mechatronics 2018;23(6):2870–80. http://dx.doi.org/10.1109/TMECH.2018.2869023.

[21] Yabui S, Inoue H, Inoue T. Control scheme of adaptive feedforward cancellation considering of bode's integral theorem for synchronous vibration suppression in rotating machineries. J. Vib. Control 2021;27(21–22):2586–99. http://dx.doi.org/10.1177/1077546320962593.

[22] Landau ID, Airimitoaie T-B, Castellanos-Silva A, Constantinescu A. Adaptive and robust active vibration control. Springer; 2016.

[23] Zaccardo VM, Buckner GD. Active magnetic dampers for controlling lateral rotor vibration in high-speed rotating shafts. Mech Syst Signal Process 2021;152:107445. http://dx.doi.org/10.1016/j.ymssp.2020.107445.

[24] Jungblut J, Haas J, Rinderknecht S. Active vibration control of an elastic rotor by using its deformation as controlled variable. Mech Syst Signal Process 2022;165:108371. http://dx.doi.org/10.1016/j.ymssp.2021.108371.

[25] DaAmato R, Amato G, Wang C, Ruggiero A. A novel tracking control strategy with adaptive noise cancellation for flexible rotor trajectories in lubricated bearings. IEEE/ASME Trans Mechatronics 2022;27(2):753–65. http://dx.doi.org/10.1109/TMECH.2021.3070890.

[26] Batista ELO, Barghouthi MR, Lopes EMdO. A novel adaptive scheme to improve the performance of feedforward active vibration control systems. IEEE/ASME Trans Mechatronics 2022;27(4):2322–32. http://dx.doi.org/10.1109/TMECH.2021.3104307.

[27] Nowak A, Campanile LF, Hasse A. Vibration reduction by stiffness modulation – A theoretical study. J Sound Vib 2021;501:116040. http://dx.doi.org/10.1016/j.jsv.2021.116040.

[28] Liu Y, Matsuhisa H, Utsuno H. Semi-active vibration isolation system with variable stiffness and damping control. J Sound Vib 2008;313(1–2):16–28. http://dx.doi.org/10.1016/j.jsv.2007.11.045.

[29] Wu Y-S, Lan C-C. Linear variable-stiffness mechanisms based on preloaded curved beams. J Mech Des 2014;136(12):122302. http://dx.doi.org/10.1115/1.4028705.

[30] Wu T-H, Lan C-C. A wide-range variable stiffness mechanism for semi-active vibration systems. J Sound Vib 2016;363:18–32. http://dx.doi.org/10.1016/j.jsv.2015.10.024.

[31] Min C, Dahlmann M, Sattel T. A concept for semi-active vibration control with a serial-stiffness-switch system. J Sound Vib 2017;405:234–50. http://dx.doi.org/10.1016/j.jsv.2017.06.007.

[32] Zhang L, Hong L, Dhupia JS, Johnson S, Qaiser Z, Zhou Z. A novel semi-active tuned mass damper with a continuously tunable stiffness. Proc Inst Mech Eng C 2023;237(2):281–93. http://dx.doi.org/10.1177/09544062221119925.

[33] Wu H, Gong N, Yang J, Gong L, Li W, Sun S. Investigation of a semi-active suspension system for high-speed trains based on magnetorheological isolator with negative stiffness characteristics. Mech Syst Signal Process 2024;208:111085. http://dx.doi.org/10.1016/j.ymssp.2023.111085.

[34] Nelson G, Rajamani R, Gastineau A, Wojtkiewicz SF, Schultz AE. Bridge life extension using semiactive vibration control. IEEE/ASME Trans Mechatronics 2015;20(1):207–16. http://dx.doi.org/10.1109/TMECH.2014.2316211.

[35] Franchek M, Ryan M, Bernhard R. Adaptive passive vibration control. J Sound Vib 1996;189(5):565–85. http://dx.doi.org/10.1006/jsvi.1996.0037.

[36] Sun C, Nagarajaiah S. Study of a novel adaptive passive stiffness device and its application for seismic protection. J Sound Vib 2019;443:559–75. http://dx.doi.org/10.1016/j.jsv.2018.12.015.

[37] Morales A, Nieto A, Chicharro J, Pintado P. Vibration isolation of unbalanced machinery using an adaptive-passive magnetoelastic suspension. J Sound Vib 2012;331(2):263–75. http://dx.doi.org/10.1016/j.jsv.2011.09.003.

[38] Turkstra T, Semercigil S. Elimination of resonance with a switching tensile support. J Sound Vib 1993;163(2):359–62. http://dx.doi.org/10.1006/jsvi.1993.1171.

[39] Turkstra T, Semercigil S. An add-on suspension for controlling the vibrations of shafts accelerating to supercritical speeds. J Sound Vib 1993;163(2):327–41. http://dx.doi.org/10.1006/jsvi.1993.1169.

[40] Suherman S, Plaut RH. Use of a flexible internal support to suppress vibrations of a rotating shaft passing through a critical speed. J Vib Control 1997;3(2):213–33. http://dx.doi.org/10.1177/107754639700300205.

[41] Wauer J, Suherman S. Vibration Suppression of Rotating Shafts Passing Through Resonances by Switching Shaft Stiffness. J Vib Acoust 1998;120(1):170–80. http://dx.doi.org/10.1115/1.2893801.

[42] Nieto A, Morales A, Chicharro J, Pintado P. Unbalanced machinery vibration isolation with a semi-active pneumatic suspension. J Sound Vib 2010;329(1):3–12. http://dx.doi.org/10.1016/j.jsv.2009.09.001.

[43] Nieto A, Morales A, Trapero J, Chicharro J, Pintado P. An adaptive pneumatic suspension based on the estimation of the excitation frequency. J Sound Vib 2011;330(9):1891–903. http://dx.doi.org/10.1016/j.jsv.2010.11.009.

[44] Zapoměl J, Ferfecki P. A computational investigation on the reducing lateral vibration of rotors with rolling-element bearings passing through critical speeds by means of tuning the stiffness of the system supports. Mech Mach Theory 2011;46(5):707–24. http://dx.doi.org/10.1016/j.mechmachtheory.2010.12.006.

[45] Hu X, Gao F, Cui C, Liu J, Wang H, Wang H, et al. Active control method for passing through critical speeds of rotating superconducting rotor by changing stiffness of the supports with use of electromagnetic force. IEEE Trans Appl Supercond 2013;23(3):5201304. http://dx.doi.org/10.1109/TASC.2012.2232699.

[46] Zhang K, Ma Y, Xiang X, Zhao W, Zhao Q. Research on transient vibration response of rotor system using supporting stiffness active control. In: 2018 joint propulsion conference. Cincinnati, Ohio: American Institute of Aeronautics and Astronautics; 2018, http://dx.doi.org/10.2514/6.2018-4823.

[47] Jin T, Liu Z, Sun S, Ren Z, Deng L, Ning D, et al. Theoretical and experimental investigation of a stiffness-controllable suspension for railway vehicles to avoid resonance. Int J Mech Sci 2020;187:105901. http://dx.doi.org/10.1016/j.ijmecsci.2020.105901.

[48] Millsaps KT, Reed GL. Reducing lateral vibrations of a rotor passing through critical speeds by acceleration scheduling. J Eng Gas Turbines Power 1998;120(3):615–20. http://dx.doi.org/10.1115/1.2818190.

[49] Blanco-Ortega A, Beltran-Carbajal F, Silva-Navarro G, Oliver-salazar M. Active vibration control of a rotorbearing system based on dynamic stiffness. Revta Fac de Ingeniería Univ de Antioquia 2010;125–33.

[50] Ding H, Li M, Fu H, Li M. The amplitude reduction of a flexible rotor passing the critical speed by modulating acceleration and stiffness simultaneously. Recent Patents Mech Eng 2018;11(3):232–41. http://dx.doi.org/10.2174/2212797611666180704145651.

[51] Lv H, Zhang S, Sun Q, Chen R, Zhang WJ. The dynamic models, control strategies and applications for magnetorheological damping systems: A systematic review. J Vib Eng Technol 2021;9(1):131–47. http://dx.doi.org/10.1007/s42417-020-00215-4.

[52] Zhu C. A disk-type magneto-rheological fluid damper for rotor system vibration control. J Sound Vib 2005;283(3):1051–69. http://dx.doi.org/10.1016/j.jsv.2004.06.031.

[53] Greiner-Petter C, Tan AS, Sattel T. A semi-active magnetorheological fluid mechanism with variable stiffness and damping. Smart Mater Struct 2014;23(11):115008. http://dx.doi.org/10.1088/0964-1726/23/11/115008.

[54] Gao P, Xiang C, Liu H, Walker P, Zhang N. Design of the frequency tuning scheme for a semi-active vibration absorber. Mech Mach Theory 2019;140:641–53. http://dx.doi.org/10.1016/j.mechmachtheory.2019.06.025.

[55] Zapoměl J, Ferfecki P, Kozánek J. Modelling of magnetorheological squeeze film dampers for vibration suppression of rigid rotors. Int J Mech Sci 2017;127:191–7. http://dx.doi.org/10.1016/j.ijmecsci.2016.11.009.

[56] Yu J, Dong X, Su X, Qi S. Development and characterization of a novel rotary magnetorheological fluid damper with variable damping and stiffness. Mech Syst Signal Process 2022;165:108320. http://dx.doi.org/10.1016/j.ymssp.2021.108320.

[57] Wang J, Liu Y, Qin Z, Ma L, Chu F. Dynamic performance of a novel integral magnetorheological damper-rotor system. Mech Syst Signal Process 2022;172:109004. http://dx.doi.org/10.1016/j.ymssp.2022.109004.

[58] Wang J, Zhang X, Liu Y, Qin Z, Ma L, Chu F. Rotor vibration control via integral magnetorheological damper. Int J Mech Sci 2023;252:108362. http://dx.doi.org/10.1016/j.ijmecsci.2023.108362.

[59] Nagaya K, Takeda S, Tsukui Y, Kumaido T. Active control method for passing through critical speeds of rotating shafts by changing stiffnesses of the supports with use of memory metals. J Sound Vib 1987;113(2):307–15. http://dx.doi.org/10.1016/S0022-460X(87)80217-1.

[60] He Y-Y, Oi S, Chu F-L, Li H-X. Vibration control of a rotor–bearing system using shape memory alloy: I. Theory. Smart Mater Struct 2006;16(1):114. http://dx.doi.org/10.1088/0964-1726/16/1/014.

[61] Borges J, Almeida A, De Araújo C, Fernandes E, Pimentel R, Aquino A. Rotor-bearing vibration control system based on fuzzy controller and smart actuators. Int J Multiphys 2013;7:197–206. http://dx.doi.org/10.1260/1750-9548.7.3.197.

[62] Enemark S, Santos IF. Rotor–bearing system integrated with shape memory alloy springs for ensuring adaptable dynamics and damping enhancement—Theory and experiment. J Sound Vib 2016;369:29–49. http://dx.doi.org/10.1016/j.jsv.2016.01.023.

[63] Ma Y, Zhang Q, Zhang D, Scarpa F, Liu B, Hong J. Tuning the vibration of a rotor with shape memory alloy metal rubber supports. J Sound Vib 2015;351:1–16. http://dx.doi.org/10.1016/j.jsv.2015.04.005.

[64] Oliveira AG, Silva AA, de Araújo CJ, Senko R, dos Reis RPB. Design and experimental analysis of a smart bearing using shape memory alloy springs. J Intell Mater Syst Struct 2020;31(11):1390–402. http://dx.doi.org/10.1177/1045389X20924829.

[65] Va'zquez JA, Barrett LE, Flack RD. A flexible rotor on flexible bearing supports: Stability and unbalance response . J Vib Acoust 2000;123(2):137–44. http://dx.doi.org/10.1115/1.1355244.

[66] Hajžman M, Balda M, Polcar P, Polach P. Turbine rotor dynamics models considering foundation and stator effects. Machines 2022;10(2). http://dx.doi.org/10.3390/machines10020077.

[67] Zeng Z, Zhang D, He T, Wang H. Experimental investigation for the dynamic mechanical properties of a vertical anisotropically supported rotor. Mech Syst Signal Process 2023;184:109678. http://dx.doi.org/10.1016/j.ymssp.2022.109678.

[68] Kang Y, Chang Y-P, Tsai J-W, Mu L-H, Chang Y-F. An investigation in stiffness effects on dynamics of rotor-bearing-foundation systems. J Sound Vib 2000;231(2):343–74. http://dx.doi.org/10.1006/jsvi.1999.2719.

[69] Cavalca K, Cavalcante P, Okabe E. An investigation on the influence of the supporting structure on the dynamics of the rotor system. Mech Syst Signal Process 2005;19(1):157–74. http://dx.doi.org/10.1016/j.ymssp.2004.04.001.

[70] Homišin J, Kaššay P, Puskar M, Grega R, Krajňák J, Urbanský M, Moravic M. Continuous tuning of ship propulsion system by means of pneumatic tuner of torsional oscillation. Int J Marit Eng 2021;158(A3). http://dx.doi.org/10.5750/ijme.v158iA3.992.

[71] Laine S, Haikonen S, Viitala R. Semi-active foundation stiffness control for rotor resonance avoidance. In: Proceedings of SIRM 2023 - the 15th European conference on rotordynamics. Darmstadt, Germany; 2023, p. 101–7. http://dx.doi.org/10.26083/tuprints-00024057.

[72] Tawfik M. Real-time vibration control of rotor-bearing system based on artificial neural networks and active support stiffness. Int J Adv Sci, Eng Inf Technol 2020;10:2305. http://dx.doi.org/10.18517/ijaseit.10.6.13377.

[73] Song LQ, Zeng LP, Zhang SP, Zhou JD, Niu HE. Design and analysis of a dual mass flywheel with continuously variable stiffness based on compensation principle. Mech Mach Theory 2014;79:124–40. http://dx.doi.org/10.1016/j.mechmachtheory.2014.04.004.

[74] Kaššay P, Grega R, Urbanský M, Krajňák J, Kačír M, Žul'ová L. Novel design of variable stiffness pneumatic flexible shaft coupling: Determining the mathematical-physical model and potential benefits. Machines 2024;12(1). http://dx.doi.org/10.3390/machines12010028.

[75] Grega R, Krajnak J, Žul'ová L, Kačír M, Kaššay P, Urbanský M. Innovative solution of torsional vibration reduction by application of pneumatic tuner in shipping piston devices. J Mar Sci Eng 2023;11(2). http://dx.doi.org/10.3390/jmse11020261.

[76] Viitala R, Viitala R. Method and device to investigate the behavior of large rotors under continuously adjustable foundation stiffness. J Vibroeng 2020;22:1037–54. http://dx.doi.org/10.21595/jve.2020.21107.

[77] Zeng Z, Zhang D, He T, Wang H. Experimental investigation for the dynamic mechanical properties of a vertical anisotropically supported rotor. Mech Syst Signal Process 2023;184:109678. http://dx.doi.org/10.1016/j.ymssp.2022.109678.

[78] Bharti SK, Bisoi A, Sinha A, Samantaray A, Bhattacharyya R. Sommerfeld effect at forward and backward critical speeds in a rigid rotor shaft system with anisotropic supports. J Sound Vib 2019;442:330–49. http://dx.doi.org/10.1016/j.jsv.2018.11.002.

[79] Muszynska A. Forward and backward precession of a vertical anisotropically supported rotor. J Sound Vib 1996;192(1):207–22. http://dx.doi.org/10.1006/jsvi.1996.0184.

[80] Genta G. Whirling of unsymmetrical rotors: A finite element approach based on complex co-ordinates. J Sound Vib 1988;124(1):27–53. http://dx.doi.org/10.1016/S0022-460X(88)81404-4.

[81] Hull EH. Shaft whirling as influenced by stiffness asymmetry. J Eng Ind 1961;83(2):219–26. http://dx.doi.org/10.1115/1.3664468.

[82] Cao H, Niu L, Xi S, Chen X. Mechanical model development of rolling bearing-rotor systems: A review. Mech Syst Signal Process 2018;102:37–58. http://dx.doi.org/10.1016/j.ymssp.2017.09.023.

[83] Xu H, Wang P, Yang Y, Ma H, Luo Z, Han Q, et al. Effects of supporting stiffness of deep groove ball bearings with raceway misalignment on vibration behaviors of a gear-rotor system. Mech Mach Theory 2022;177:105041. http://dx.doi.org/10.1016/j.mechmachtheory.2022.105041.

[84] Ma S, Yin Y, Chao B, Yan K, Fang B, Hong J. A real-time coupling model of bearing-rotor system based on semi-flexible body element. Int J Mech Sci 2023;245:108098. http://dx.doi.org/10.1016/j.ijmecsci.2022.108098.

[85] Zhang X, Han Q, Peng Z, Chu F. A comprehensive dynamic model to investigate the stability problems of the rotor–bearing system due to multiple excitations. Mech Syst Signal Process 2016;70–71:1171–92. http://dx.doi.org/10.1016/j.ymssp.2015.10.006.